EVS38
Göteborg, Sweden, June 15-18, 2025

New Fast Charging Protocols minimizing Lithium plating based on Electrochemical-Thermal-Life model for Lithium-Ion Batteries

Song-Yul Choe[1]*, Kyungjin Yu[1], Adekanmi Miracle Adeyinka[1],Wooju Lee[2]

[1]Department of Mechanical Engineering, Auburn University, USA

[2]Hyundai Motor Company, 150, Hyundaiyeonguso-ro, Namyang-eup, Hwaseong-si, Gyuonggi-do, Republic of Korea

*Corresponding Author: Mechanical Engineering, Auburn University, 1418 Wiggins Hall, Auburn, AL 36849, USA. Email: choe@auburn.edu. Tel: 334-844-3328

Executive Summary

Long charging time is one of the barriers that should be overcome to increase the acceptance of electric vehicles in the market drastically. The charging time can be simply reduced by increasing the charging current, which significantly reduces lifespan, generates more heat, and deteriorates the safety of batteries. Therefore, currently widely used Multi-Constant Current (MCC) fast-charging methods are optimized using a reduced-order electrochemical life model that considers thermal, aging, and safety aspects. First Optimal MCC (O-MCC) charging protocol can suppress Lithium Plating (LiP) over cycle life based on the battery's State of Health (SOH). Then, the O-MCC protocol is further optimized using negative pulses (O-MCC+NP) that simultaneously suppresses LiP and recovers lithium-ions out of any plated lithium via lithium stripping (LiS). The optimization of the parameters for current profiles are carried out using Nonlinear Model Predict Control (NMPC) algorithms. The results of the proposed new charging protocols are experimentally tested and compared with commercial charging protocols, showing reduced charging time with a prolonged lifetime.

Keywords: Fast charging, Lithium-ion battery, Lithium plating, Lithium stripping, Electrochemical thermal-life model.

1. Introduction

The widespread adoption of electric vehicles (EVs) and the increasing number of portable electronic devices have triggered the need for more efficient, reliable, and durable use of lithium-ion batteries (LiBs). Despite significant advancements in LiB technology, the demand for fast charging (FC) and prolonged battery life remains a challenge. A simple approach to reducing the charging time is to increase the charging current rate; however, this leads to accelerated aging and an increased heat generation rate (HGR) [1], [2]. The additional heat produced not only diminishes the system's energy efficiency but also results in higher operating temperatures, necessitating the design and implementation of an enlarged cooling system to manage the temperature effectively.

When designing fast charging protocols, it is crucial to consider the battery lifespan to ensure the cycle and calendar life warranty. The dominant causes of aging during charging are electrochemical degradation such as Side Reactions (SR) and Lithium Plating (LiP). SR is the inevitable reaction between lithium ions and solvents in the electrolyte, which products form a layer called Solid Electrolyte Interphase (SEI) at the surface of the anode particles. LiP is another reaction of lithium ions with electrons that forms a solid lithium layer at the surface of the anode particles. Additionally, as charging and discharging continue, mechanical degradation can occur due to the change of ion concentrations in the solid, which causes repeated expansion and contraction, potentially leading to cracks and fractures. These result in loss of active material, loss of lithium inventory,

dryness of electrolytes and growth of SEI and increases Lithium plating , which ultimately drops the battery's capacity and power [3], [4].

The Multi-stage Constant Current (MCC) protocol has widely gained popularity in the industry due to its easy implementation via a lookup table (LUT) [5]. However, the performance of MCC protocols highly depends on the current amplitude at each stage and the criteria for transitioning between stages. Although LiP onset conditions are often considered when determining the amplitude and transitions of stages [6], accurate prediction of LiP occurrence is not possible because the continuously varying reaction mechanisms inside the cell are affected by operating conditions.

Several researchers have proposed hybrid methods that combine MCC with Negative Pulse (NP) protocols that consider the effects of thermal and degradation. Monem et al. experimentally compared various charging protocols, including CC/CV, CC/CV+NP, MCC/CV, and MCC/CV+NP, with different NP frequencies [7], [8]. Song et al. proposed an MCC+NP protocol, where the charging current was reduced to avoid LiP, using SOC-based stage transitions. However, the discharging current was fixed at 2C at 20mHz frequency to promote LiS without optimization [9]. Yin et al. proposed an MCC+NP protocol that optimized the charging current based on the degradation rate and maximum concentration, with NP parameters optimized to promote LiS when LiP occurs [10]. Although more NP were applied to promote LiS, the protocol did not constrain the LiP. Additionally, the effects of NP on heat generation and resistance increase were not addressed.

This paper introduces two new optimal fast charging (FC) protocols that balance the charging speed, heat generation, and battery health within the safe operation range predicted by an electrochemical thermal life model of LiBs. The first protocol, Optimized MCC (O-MCC), focuses on minimizing the charging time, while the second protocol, O-MCC+NP, incorporates a negative pulse (NP) into the protocol that further enhances the charging efficiency and mitigates lithium plating. Both protocols are designed to adapt dynamically to the battery's state of charge and temperature, ensuring optimal performance throughout the charging process.

2. Concept of the proposed system

The schematic diagram of the overall concept for the proposed charging protocol is depicted in **Figure 1** which includes a battery and an electrochemical thermal life model that runs in parallel, a Kalman filter that corrects the model errors and an NMPC to determine the optimal parameters of the charging protocols.

The electrochemical thermal life model is an important part of the system that represents the dynamics of lithium ions, such as ion transport, electrochemical kinetics, energy balance, and degradation processes during charging and discharging. The model is described by a combination of nonlinear partial differential equations, which are collectively known as the Full Order Model (FOM). It provides detailed responses of the internal variables but is computationally intensive and unsuitable for real-time control applications. Therefore, the equations are mathematically simplified, which is referred to as the Reduced Order Model (ROM) to balance computational efficiency and accuracy. ROMs can be categorized into Pseudo-Two-Dimensional (P2D) and Single Particle Model (SPM) based on the assumptions of the particle number. Even though SPM drastically reduces computational time, degradation caused by the gradient internal variables across the thickness direction cannot be represented, which is particularly required in the anode electrode for accurate aging prediction. Consequently, P2D was chosen as the anode to reflect better aging prediction. However, SPM is still used for the composite cathode due to the computational time. The resulting hybridized ROM is called the P2D-SPM. The details of the P2D-SPM are provided in references [10], [11]. The thermal model calculates the heat generation rate (HGR) of the cell based on the energy balance equation, and the degradation model calculates the side reaction (SR) and lithium plating (LiP) reaction rates based on the Butler-Volmer equations [12], [13]. However, the real-time calculation of the algorithms still takes too long, and therefore, the protocols derived from P2D-SPM are converted into a look-up table (LUT) and implemented in a battery-in-the-loop.

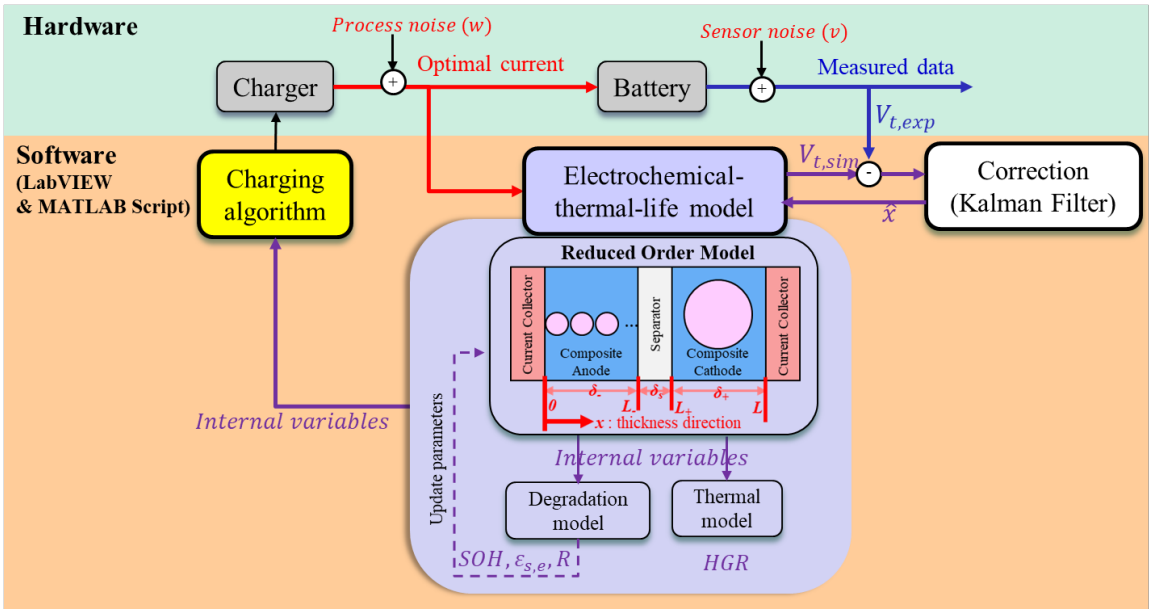

Figure 1 Schematic diagram of the overall concept.

3. Experimental

The experimental study was conducted using commercial lithium-ion pouch cells with a nominal capacity of 25.9 Ah along the voltage range of 2.5-4.15V The cell chemistry is NMC811 with graphite.

A test station was constructed, and the experiments were conducted at 25 °C isothermal conditions using a recently developed multifunctional calorimeter that regulates the desired cell temperature through a feedback control loop, implemented in LabVIEW® software, dynamically adjusts the Peltier current to maintain the temperature within a 0.1 °C error tolerance. A heat flux sensor was selected to measure the HGR due to its high sensitivity and measurable range of ±150 kW/m². The Peltier cells were controlled using a bipolar power supply, which enabled heating and cooling functions.

Before starting the measurements, a uniform compressive pressure of 25 kPa was applied to the pouch cell. The experimental procedure involved 2C CC charge, 3C CC charge, and MCC charge protocols, each followed by a 1C CC discharge. The 2C and 3C CC tests were conducted from an SOC of 0% up to the cut-off voltage, whereas the SOC range for the MCC was consistently set between 9.7% and 77.6%. The capacity was measured every 50 cycles using a C/3 CC discharge and repeated until the capacity fade reached 80% of the fresh cell, which is considered the End of Life (EoL).

4. Model validation

The reduced order electrochemical-thermal life model was validated with 2C CC charge, 3C CC charge, and MCC charge protocols with 1C CC discharge. The results are shown in Figure 2. Figure 2 (a) shows the state of health (SOH) across the cycle life. Under the 2C CC profile, the capacity degradation exhibited a linear trajectory, largely governed by side reactions. In contrast, 3C CC and MCC protocols have revealed a nonlinear degradation, which is attributed to the increasing influence of lithium plating. Notably, MCC charging leads to a significant drop in capacity beyond 150 cycles, indicating a transition to accelerated degradation.

As the cell ages, the CC protocols inherently reduce the charging time due to the decreasing maximum achievable SOC. However, the MCC maintains a constant SOC range, resulting in progressively longer charging durations with cycle aging. Given that electric vehicle manufacturers often define charging performance based

on a fixed SOC window (e.g., 10–80% SOC in 30 min), the implications of extended charging time under MCC are significant and should be considered during protocol development.

Figure 2 (b) and (c) show the Root Mean Squared Error (RMSE) between the simulated and experimental data, which remains within an acceptable range from BoL to EoL. The voltage RMSE values remain below 35 mv, and capacity RMSE values are within 0.4 Ah across all protocols. These results validate the accuracy of the model in predicting both terminal voltage and capacity fade under various cycling conditions. Figure 2 (d) and (e) show the MCC charging current and voltage responses at the BoL, Middle of Life (MoL), and EoL. The MCC protocols were determined by considering the LiP overpotential at BoL. The maximum C-rate is set to 2.6C and then reduced by C/2 when it reaches a preset LiP overpotential of 0.02V or the cut-off voltage. When the terminal voltage reached the cutoff voltage three times, the C-rate was reduced by C/3. As the cell ages, the terminal voltage increases faster and reaches the cut-off voltage, so the amplitude of the MCC decreases earlier. As a result, the charging time becomes longer.

Figure 2 (f) shows the HGR by experiment and simulation until EoL. As the cell ages, the HGR increases significantly due to the increased internal resistance. The RMSE was less than 4 W. The increased internal resistance not only affects the charging time but also affects the energy efficiency of the cell. This phenomenon leads to a reduction in the cell's capacity and its ability to deliver power effectively. Figure 2 (g) shows the calculated LiP overpotential at the particle close to the separator, which shifts downward as the cell ages. This downward shift in LiP overpotential indicates a reduction in the driving force for lithium intercalation as the cell degrades. The decrease in intercalation kinetics contributes to the overall capacity fade and performance degradation observed in aged cells.

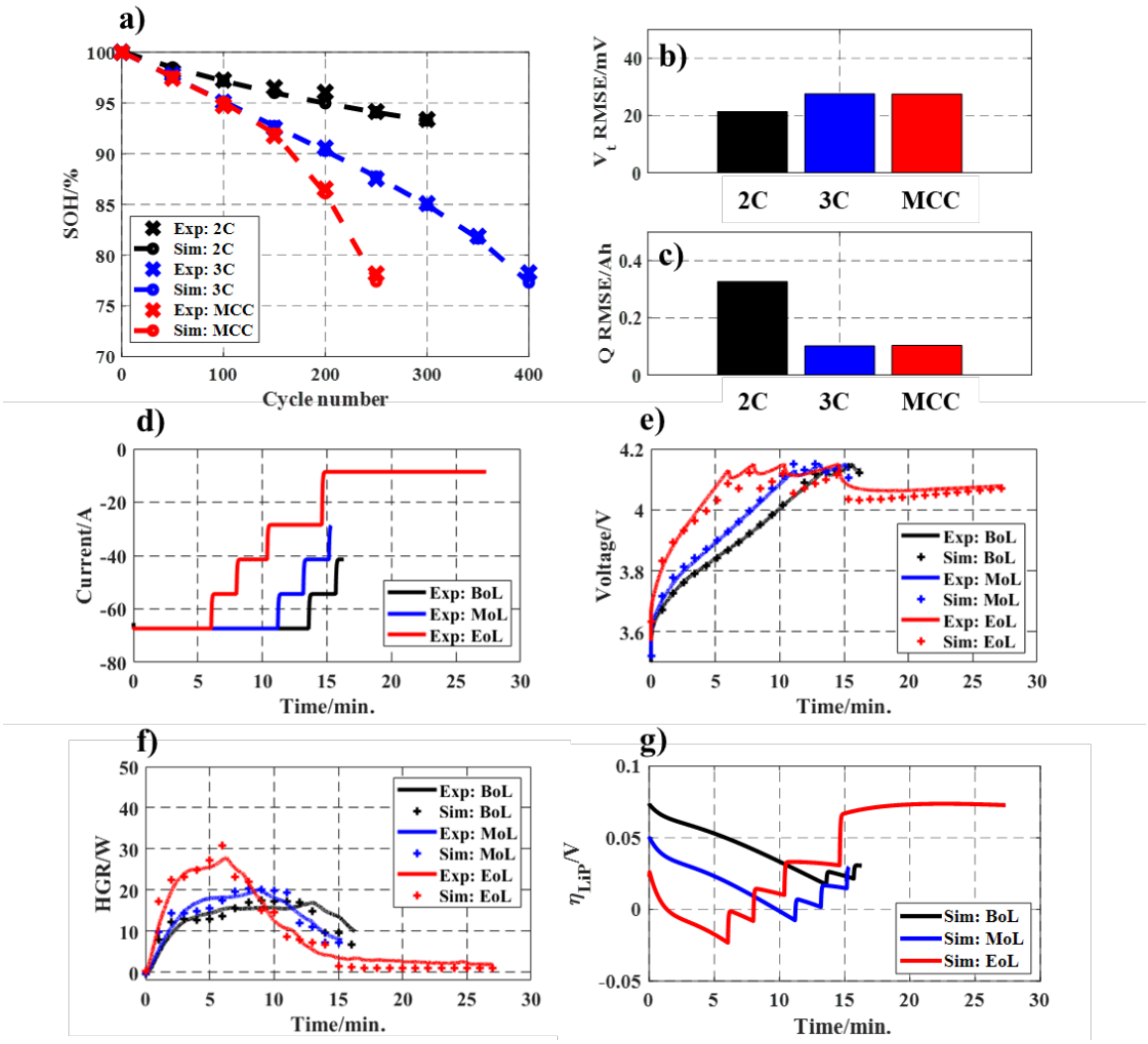

Figure 2. Model validation results under 2C, 3C, and MCC: a) SOH, b) Voltage RMSE, and c) Capacity RMSE. Model validation results under MCC profile throughout life; d) Current, e) Voltage, f) HGR, and g) LiP overpotential at the nearest particle to the separator.

4.1 Optimization of Fast Charging (FC) multi-stage constant current (MCC) protocols

The O-MCC protocol consists of a stepped current pattern with multiple CC stages. The current amplitude and stage transition points significantly affect the cell performance, which are optimized using the NMPC algorithm to minimize the two objective functions of charging time and degradation within a limited Heat Generation Rate (HGR) [14]. The LiP was predicted using the LiP overpotential. The onset of the reaction occured when the overpotential was less than 0V. The suppression of the reaction is controlled by constraining the LiP overpotential between 0.02V to 0.03V with a margin of 0.02V away from the critical condition of 0V.

The optimisation of the charging problem is formulated with objective functions which minimize the charging current, thus reducing the charging time. The constraints include current, voltage, SOC, LiP overpotential, and constant current time (t_{cc}), which are defined as follows:

$$
\begin{aligned}
& J = \min_{I}\left(\sum_{t}^{t+N_h} I\right) \\
& -5C \le I \le -C/3 \\
& 2.5V \le V_t \le 4.15V \\
& 9.7\% \le SOC \le 77.6\% \\
& 0.02V \le \eta_{LiP} \le 0.03V \\
& t_{cc} \ge 60\,\text{sec}
\end{aligned}
\qquad \textit{Eq. 1}
$$

The optimal control problem was implemented using a *'fmincon'*, which is a built-in MATLAB function. Sequential Quadratic Programming (SQP) was chosen as the solver because of its robustness and effective constraint handling.

The O-MCC protocol was implemented in the testing environment using a voltage and SOH-based LUT to verify its performance with easy adaptability. First, the O-MCC protocol is derived offline using the electrochemical thermal life model and then used to generate the voltage and SOH-based LUT for experimental implementation. The cell voltage measured in real-time was used to determine the current amplitude from the LUT, and the capacity measured every 50 cycles was used to update the LUT based on the SOH.

The performance of the O-MCC protocol was experimentally validated through a cycling life test until EoL and compared with MCC, which is a voltage-based LUT. In addition, O-MCCs with different constraints were proposed to meet different demands regarding charging time, degradation, and HGR.

Figure 3 (a) and (b) show the current and voltage profiles of the various charging protocols. The charging time by MCC takes 16min from 9.7 % to 77.6 % SOC, while the charging time by O-MCC (A) is 14min., which is 11.7 % shorter. Figure 3 (c) shows the SOH over cycle number by MCC and O-MCC (A) in black and blue, respectively, whereas the simulation and experimental data are plotted with dashed lines and 'x' marks. The SOH by MCC and O-MCC (A) reached EoL after 250 and 700 cycles, respectively, where O-MCC (A) extended by 450 more cycles. The capacity of MCC decreased nonlinearly starting from the 150th cycle. Capacity loss by LiP begins to occur from 200 cycles to EoL, as shown in Figure 3 (d), as the LiP overpotential falls below 0V starting from MoL (Figure 2 g). Similarly, the capacity loss due to SR is the only mechanism present in O-MCC(A), because the LiP overpotential is maintained within the preset tolerance and no LiP reaction takes place.

The charging times at BoL, MoL, and EoL are shown in Figure 3 (e). The results showed that the charging times from BoL to EoL by both MCC and O-MCC (A) increased. When cells get aged, the internal resistance increases, and the terminal voltage increases rapidly. Consequently, the MCC reaches the transition point earlier and reduces the current amplitude to the next stage, resulting in an increased charging time. However, the current amplitude by O-MCC is reduced as a function of SOH while satisfying the LiP overpotential constraint, which subsequently increases the charging time. At EoL, the charging time of O-MCC (A) was longer than that of MCC.

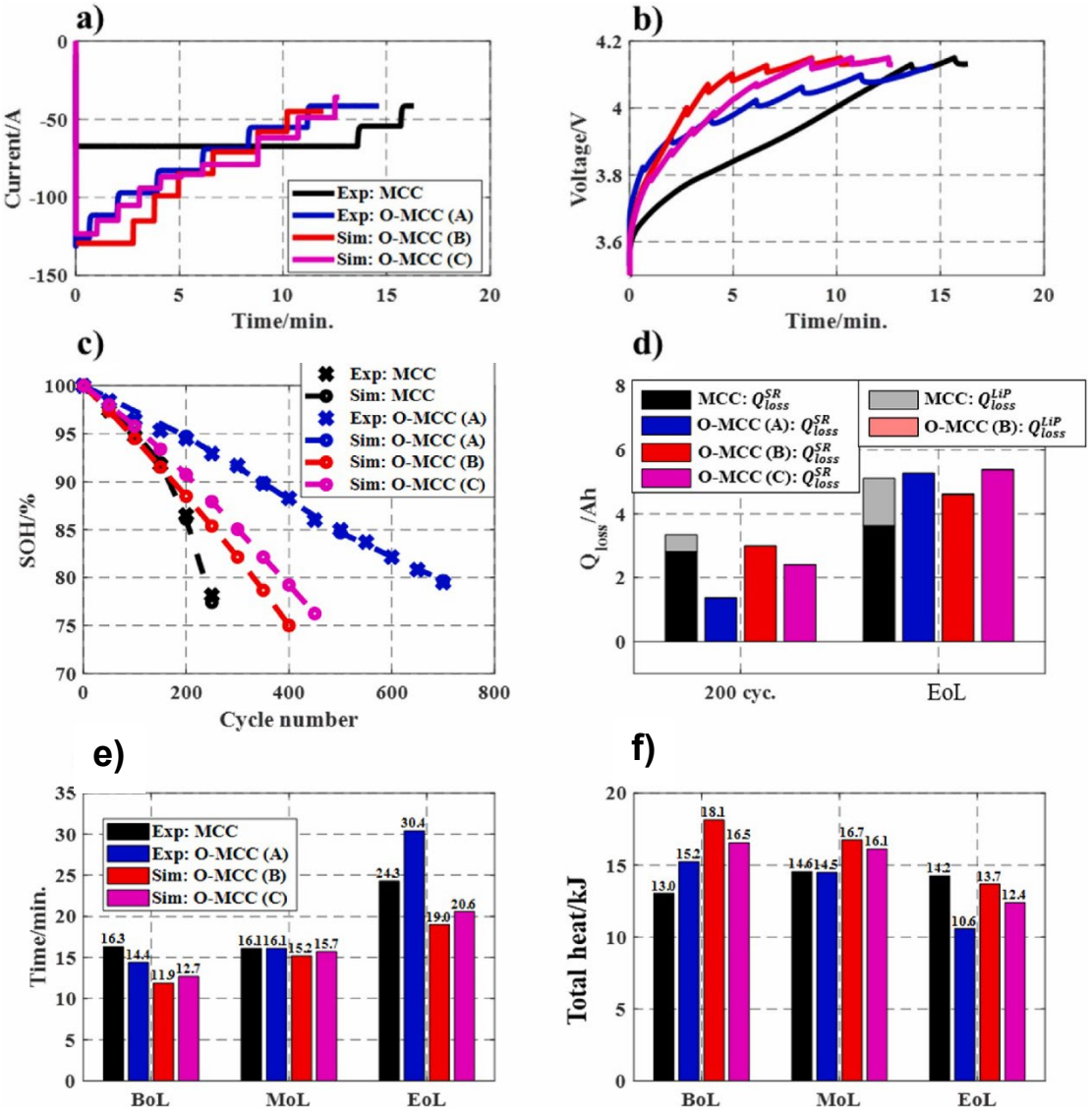

Figure 3 Comparison of FC protocols: a) Current, b) Voltage, c) SOH, d) Source of capacity loss, e) Charging time, and f) Total heat.

Figure 3 (f) shows the total heat generation during charging at BoL, MoL, and EoL, obtained by integrating the HGR over time. Since the HGR is proportional to the charging current amplitude, the faster the charging protocol is, the more heat is generated. The heat generated by O-MCC (A) is smaller at EoL than that generated by MCC because of the reduced current amplitude for aged cells.

4.2Optimized MCC with negative pulse (O-MCC+NP) protocol

The first O-MCC proposed wass further improved by adding a series of NPs to the MCC protocol to promote Lithium Stripping (LiS) that recovers lithium ions from the plated lithium. As a result, the margin of the LiP was reduced and the LiP overpotential lower limit was set to 0V. Additionally, concentration gradients in solids are

considered a constraint for LiP because the concentration gradient between the anode particle surface and inside accelerates LiP.

Similarly, the optimal charging problem is formulated with objective functions to minimize the charging current and time. The control and prediction horizons N_c were set to 47 sec. in relation to the charging time t_c, which implies that the charging current is optimized while maintaining constraints considering the performance of the next 47sec. The constraints include the current, SOC, LiP overpotential, and ion concentration difference between the surface and the average of the anode particle near the separator, defined as follows:

$$
\begin{aligned}
& I_{c,opt}(t) = \underset{I_c \in [-5C,-C/3]}{\arg\min} \left(\sum_{t}^{t+N_c} I_c \right) \\
& -5C \le I \le -C/3 \\
& 9.7\% \le SOC \le 77.6\% \\
& \eta_{LiP,L_-} \ge 0V \\
& \left(c_{s,surf} - c_{s,ave} \right)_{L_-} \le 7.5 \times 10^{-3} \, mol/cm^3
\end{aligned}
\qquad \text{Eq. 2}
$$

, where the maximum charging rate is limited to 5C to prevent excessive heat generation that can potentially damage cell materials due to hot spots and the effects of mechanical stress caused by high C-rates [15]. The minimum charging rate was limited to C/3, considering the charging time [9]. The SOC range was set between 9.7% and 77.6% for comparison with MCC. The ion concentration difference between the surface and average of the anode particles near the separator was also constrained. Its maximum value was obtained by model-based analysis, considering that the LiP onset point occurs when the ion concentration difference reaches $(8 \pm 0.5) \times 10^{-3}$ mol/cm^3. Moreover, the limited solid concentration gradient possibly reduces particle stress, which leads to mechanical degradation [16], [17].

In addition, the discharging current was optimized using the same method, where the control and prediction horizons N_d were set to 3sec., corresponding to the discharging time t_d. These constraints include the current, voltage, and LiP and LiS reaction rate, defined as follows:

$$
\begin{aligned}
& I_{d,opt}(t) = \underset{I_c \in [1C,2C]}{\arg\min} \left(\sum_{t}^{t+N_d} I_d \right) \\
& 1C \le I \le 2C \\
& V_t \le 4.1V \\
& j_{LiP,L_-} \le j_{LiS,L_-}
\end{aligned}
\qquad \text{Eq. 3}
$$

, where the range of the discharging current rate is determined between 1C and 2C, which are obtained from experimental case studies on NP amplitude. Voltage is constrained to remain under 4.1V to reduce voltage polarization and delay the CV mode, which would otherwise extend charging time. The LiP reaction rate was constrained to be smaller than that of LiS to recover as many lithium ions out of the plated lithium as possible.

The parameters for the incorporated negative pulse were the frequency and the amplitude determined by experimental studies on both the charging time and HGR. It turned out that a 20mHz pulse significantly reduces HGR with a minimum increase in charging time. The amplitudes of the charging and discharging currents were optimized using two separate NMPC algorithms, with a focus on minimizing the charging time and degradation. Finally, the proposed O-MCC+NP protocol was obtained and implemented in the Battery-In-the-Loop (BIL) system, which facilitates prediction, correction, and optimization of different internal variables in real time.

Figure 5 (a) shows SOH versus cycle number throughout EoL. The cycle life of O-MCC+NP was prolonged up to 400 cycles, increasing by 150 cycles more than that of MCC. At 200 cycles, O-MCC+NP reduced the capacity loss by 37.3% and 16% reduction in charging time compared to MCC. The capacity loss

by MCC is induced by LiP, leading to a rapid nonlinear capacity drop, whereas O-MCC+NP suppresses LiP at 200 cycles.

Figure 5 (b) shows the charging time of the two charging protocols at BoL, MoL, and EoL compared to the conventional MCC protocol. At BoL, the charging times of MCC, O-MCC, and O-MCC+NP are 16.3 min., 14.3 min., and 13.6 min. At EoL, the charging time increased for all charging protocols considered. However, the charging time for the O-MCC+NP protocol at EoL was the lowest because of the upshifted LiP overpotential and reduced concentration gradient.

These two approaches have pros and cons. For simple implementation, O-MCC is a better choice; however, the charging time of O-MCC significantly increases up to 30min at EoL using the classical overpotential with a margin greater than 0.02V. If the design criteria are set to reduce the charging time, O-MCC+NP is the better choice because of the optimally reduced charging time throughout the life without LiP, where the margin of the LiP potential should be set to 0V. Even though LiP does not occur, the capacity fade is severe because of the higher C-rates and associated side reactions. With respect to safety, the LiP is the criterion to be considered.

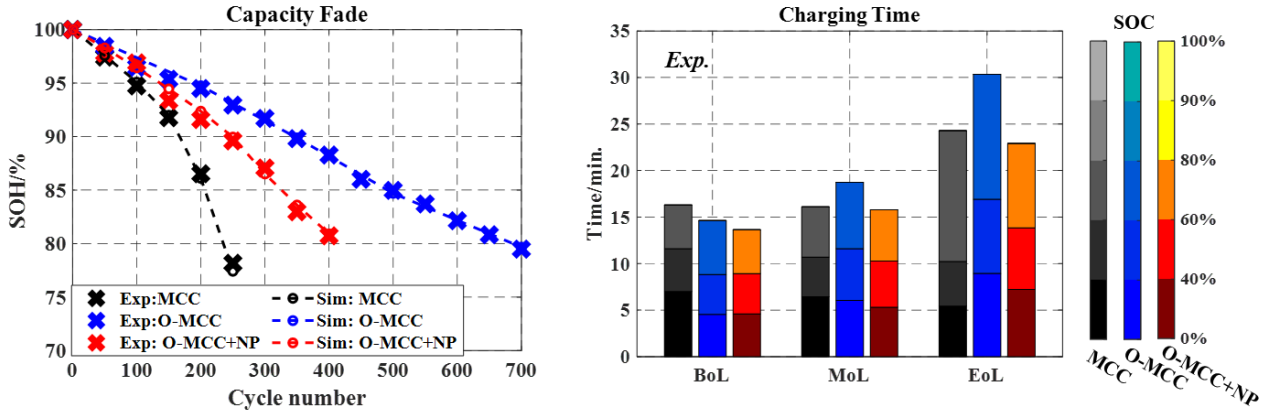

Figure 4 Experimental and simulation results: (a) SOH (b) charging time analysis for MCC, O-MCC and O-MCC +NP.

5. Conclusion

In this study, two new FC protocols based on the current fast charging protocol, O-MCC and O-MCC+NP, are proposed that consider aging and thermal effects of LiBs based on the validated reduced electrochemical thermal life model. O-MCC can suppress LiP as SOH decreases. The current magnitudes of each MCC stage and their transition points are optimized using NMPC and converted into voltage and SOH-based LUT for simple implementation. Conversely, O-MCC+NP includes intermediate discharging pulses to facilitate LiS out of plated lithium. The current amplitudes were optimized using NMPC algorithms, and the frequency of the NP was determined experimentally, which reduced the heat generation term through diffusion resistance.

The O-MCC+NP was implemented in the BIL system and runs in real-time. The proposed O-MCC and O-MCC+NP charging protocols were experimentally tested and compared with a commercial MCC charging protocol. The results showed 59% and 37% reductions in capacity loss, with 12% and 16% reductions in charging time, respectively. The charging time by O-MCC+NP was further reduced than that by O-MCC by minimizing the margin of LiP overpotential with the concept that any unexpected formation of LiP can be cured by LiS. However, the capacity loss of the O-MCC might be smaller than that of O-MCC+NP if the overpotential margin for LiP increases.

The O-MCC and O-MCC + NP protocols demonstrated a trade-off between charging speed and capacity retention. These advanced charging methods offer significant improvements over commercial MCC protocols, allowing users to prioritize faster charging or a longer battery life. Future research could focus on enhancing the fast charging algorithm by considering other degradation mechanisms, evaluating performance under different temperature conditions, exploring applicability across different battery chemistries, and extending the validation to pack-level implementations.

Nomenclature

Nomenclature			Abbreviations	
c_s	mol cm^{-1}	Concentration	BIL	Battery-in-the-Loop
I	A	Current	BoL	Beginning of Life
$N_{c/d}$	Sec.	NMPC prediction and control horizon length	CC	Constant Current
Q_{max}	Ah	Maximum cell capacity	CV	Constant Voltage
t	Sec.	Time	EoL	End of Life
U_{OC}	V	Open circuit voltage	EV	Electric Vehicle
U_{eq}	V	Equilibrium potential	FC	Fast Charging
V_t	V	Terminal voltage	FOM	Full-order Electrochemical Model
η	V	Overpotential	HGR	Heat Generation Rate
			LiP	Lithium Plating
Abbreviations			LiS	Lithium Stripping
O-MCC+NP	Optimized Multi-stage Constant Current with Negative Pulse		LUT	Look-Up Table
P2D	Pseudo Two Dimensional		NMPC	Nonlinear Model Predictive Control
RMSE	Root Mean Squared Error		NMC	Nickel Manganese Cobalt
ROM	Reduced-Order Electrochemical Model		NP	Negative Pulse
SOC	State of Charge		MCC	Multi-stage Constant Current
SOH	State of Health		MoL	Middle of Life
SEI	Solid Electrolyte Interphase		OCV	Open Circuit Voltage
SPM	Single Particle Model		O-MCC	Optimized Multi-stage Constant Current
SR	Side Reaction			

Reference

[1] M. Song and S.-Y. Choe, "Fast and safe charging method suppressing side reaction and lithium deposition reaction in lithium ion battery," *J. Power Sources*, vol. 436, p. 226835, Oct. 2019, doi: 10.1016/j.jpowsour.2019.226835.

[2] M. Song, M. Choi, and S.-Y. Choe, "Start-Up Charging Strategy for a Large-Format NMCA/Graphite Pouch Cell from Subzero Temperature Using an Electrochemical, Thermal, and Mechanical Life Model," *J. Electrochem. Soc.*, vol. 170, no. 6, p. 060533, Jun. 2023, doi: 10.1149/1945-7111/acdd1f.

[3] X. Zhao, Y. Bi, S.-Y. Choe, and S.-Y. Kim, "An integrated reduced order model considering degradation effects for LiFePO4/graphite cells," *Electrochimica Acta*, vol. 280, pp. 41–54, Aug. 2018, doi: 10.1016/j.electacta.2018.05.091.

[4] R. Fu, S.-Y. Choe, V. Agubra, and J. Fergus, "Development of a physics-based degradation model for lithium ion polymer batteries considering side reactions," *J. Power Sources*, vol. 278, pp. 506–521, Mar. 2015, doi: 10.1016/j.jpowsour.2014.12.059.

[5] M. Usman Tahir, A. Sangwongwanich, D.-I. Stroe, and F. Blaabjerg, “Overview of multi-stage charging strategies for Li-ion batteries,” *J. Energy Chem.*, vol. 84, pp. 228–241, Sep. 2023, doi: 10.1016/j.jechem.2023.05.023.
[6] I. A. Shkrob, M.-T. F. Rodrigues, and D. P. Abraham, “Fast Charging of Li-Ion Cells: Part V. Design and Demonstration of Protocols to Avoid Li-Plating,” *J. Electrochem. Soc.*, vol. 168, no. 1, p. 010512, Jan. 2021, doi: 10.1149/1945-7111/abd609.
[7] M. Abdel Monem *et al.*, “Lithium-ion batteries: Evaluation study of different charging methodologies based on aging process,” *Appl. Energy*, vol. 152, pp. 143–155, Aug. 2015, doi: 10.1016/j.apenergy.2015.02.064.
[8] M. Abdel-Monem, K. Trad, N. Omar, O. Hegazy, P. Van den Bossche, and J. Van Mierlo, “Influence analysis of static and dynamic fast-charging current profiles on ageing performance of commercial lithium-ion batteries,” *Energy*, vol. 120, pp. 179–191, Feb. 2017, doi: 10.1016/j.energy.2016.12.110.
[9] M. Song and S.-Y. Choe, “Fast and safe charging method suppressing side reaction and lithium deposition reaction in lithium ion battery,” *J. Power Sources*, vol. 436, p. 226835, Oct. 2019, doi: 10.1016/j.jpowsour.2019.226835.
[10] Y. Yin and S.-Y. Choe, “Actively temperature controlled health-aware fast charging method for lithium-ion battery using nonlinear model predictive control,” *Appl. Energy*, vol. 271, p. 115232, Aug. 2020, doi: 10.1016/j.apenergy.2020.115232.
[11] Y. Yin, Y. Hu, S.-Y. Choe, H. Cho, and W. T. Joe, “New fast charging method of lithium-ion batteries based on a reduced order electrochemical model considering side reaction,” *J. Power Sources*, vol. 423, pp. 367–379, 2019.
[12] X. Zhao, Y. Yin, Y. Hu, and S.-Y. Choe, “Electrochemical-thermal modeling of lithium plating/stripping of Li(Ni0.6Mn0.2Co0.2)O2/Carbon lithium-ion batteries at subzero ambient temperatures,” *J. Power Sources*, vol. 418, pp. 61–73, Apr. 2019, doi: 10.1016/j.jpowsour.2019.02.001.
[13] A. M. Adeyinka, K. Yu, S.-Y. Choe, and W. Lee, “Thermal Characterization of Lithium-Ion Batteries under Varying Operating Conditions,” SAE International, Warrendale, PA, SAE Technical Paper 2024-01–2667, Apr. 2024. doi: 10.4271/2024-01-2667.
[14] K. Yu, A. M. Adeyinka, S.-Y. Choe, and W. Lee, “Optimized multi-stage constant current fast charging protocol suppressing lithium plating for lithium-ion batteries using reduced order electrochemical-thermal-life model,” *J. Power Sources*, vol. 626, p. 235759, Jan. 2025, doi: 10.1016/j.jpowsour.2024.235759.
[15] K. An, P. Barai, K. Smith, and P. P. Mukherjee, “Probing the Thermal Implications in Mechanical Degradation of Lithium-Ion Battery Electrodes,” *J. Electrochem. Soc.*, vol. 161, no. 6, p. A1058, May 2014, doi: 10.1149/2.069406jes.
[16] M. Song, M. Choi, and S.-Y. Choe, “Start-Up Charging Strategy for a Large-Format NMCA/Graphite Pouch Cell from Subzero Temperature Using an Electrochemical, Thermal, and Mechanical Life Model,” *J. Electrochem. Soc.*, vol. 170, no. 6, p. 060533, Jun. 2023, doi: 10.1149/1945-7111/acdd1f.
[17] J. Li, K. Adewuyi, N. Lotfi, R. G. Landers, and J. Park, “A single particle model with chemical/mechanical degradation physics for lithium ion battery State of Health (SOH) estimation,” *Appl. Energy*, vol. 212, pp. 1178–1190, Feb. 2018, doi: 10.1016/j.apenergy.2018.01.011.

Presenter Biography

S.-Y. Choe is an endowed professor with the Department of Mechanical Engineering, Auburn University. Before joining Auburn University, he was the director of the HEV and EV program of Hyundai Kia Motor Company. His current research focuses on theoretical and experimental investigations of electrochemical devices such as fuel cells and batteries.